Deep Sea Research Part I: Oceanographic Research Papers
February 2018, Volume 132, Pages 29-36
http://dx.doi.org/10.1016/j.dsr.2017.12.005
http://archimer.ifremer.fr/doc/00418/52971/

Deep-towed high resolution seismic imaging II: Determination of P-wave velocity distribution

Marsset Bruno [1, *], Ker Stephan [1], Thomas Yannick [1], Colin Florent [1]

[1] Ifremer, REM/GM/LAD, Centre de Brest, BP 70, 29280 Plouzane, France

* Corresponding author : Bruno Marsset, email address : Bruno.Marsset@ifremer.fr

Abstract :

The acquisition of high resolution seismic data in deep waters requires the development of deep towed seismic sources and receivers able to deal with the high hydrostatic pressure environment. The low frequency piezoelectric transducer of the SYSIF (SYstème Sismique Fond) deep towed seismic device comply with the former requirement taking advantage of the coupling of a mechanical resonance (Janus driver) and a fluid resonance (Helmholtz cavity) to produce a large frequency bandwidth acoustic signal (220–1050 Hz). The ability to perform deep towed multichannel seismic imaging with SYSIF was demonstrated in 2014, yet, the ability to determine P-wave velocity distribution wasn't achieved. P-wave velocity analysis relies on the ratio between the source-receiver offset range and the depth of the seismic reflectors, thus towing the seismic source and receivers closer to the sea bed will provide a better geometry for P-wave velocity determination. Yet, technical issues, related to the acoustic source directivity, arise for this approach in the particular framework of piezoelectric sources. A signal processing sequence is therefore added to the initial processing flow. Data acquisition took place during the GHASS (Gas Hydrates, fluid Activities and Sediment deformations in the western Black Sea) cruise in the Romanian waters of the Black Sea. The results of the imaging imagingimaiaging processing are presented for two seismic data sets acquired over gas hydrates and gas bearing sediments. The improvement in the final seismic resolution demonstrates the validity of the velocity model.

Highlights

► Perform deep towed High Resolution velocity determination. ► Increase seismic imaging performance. ► Bottom simulating Reflecto.

Keywords : Deep-towed seismic, seismic imaging, P-wave velocity distribution

I. INTRODUCTION

High Resolution (220-1050 Hz) seismic acquisition performed in great water depth using deep-towed systems provides unrivalled lateral resolution when compared to conventional surface seismic methods (50-250 Hz, Chapman et al., 2002; Gettrust et al., 2004). This gain in lateral resolution is primarily related to the acquisition geometry as it decreases the width of the first Fresnel zone. The gain also depends on the processing sequence in which imaging algorithms (migration) improve the resolution down to the mean wavelength of the seismic signal. Yet this ideal resolution may only be obtained if the correct velocity model is used. This requires the determination of the fine scale P-wave velocity distribution.

In a general case, P-wave velocities in shallow marine sediments are not expected to display strong variations due to the relative homogeneity of the medium. However, in the presence of existing fluid systems including the existence of gas or/and gas hydrates, the P-wave velocity distribution can vary significantly both laterally and vertically, making quantifying the velocity distribution (e.g., Helgerud et al, 1999) a key factor in gas/gas hydrate saturation assessment (He et al, 2009).

A large number of methods are available to access to the seismic velocity distribution. These methods differ according to their initial hypothesis, from the simplest (flat horizontal reflectors, Pythagorean theorem) to the most complex (calculation of the Green functions in a complex medium), yet they all rest on the accuracy of the source-receiver positions which remains the key point of any seismic acquisition.

The US NRL (Naval Research Laboratory) DTAGS (Deep Towed Acoustics Geophysics System) has successfully determined P-wave velocity distribution and thus acoustically characterized the medium (Wood et al., 2003, 2008). Nevertheless, the DTAGS pre-stack processing approach rests on the use of "Super Gather", up to 300 m-large and therefore the resulting smearing of information limits the accuracy for the determination of fine-scale P-wave velocity models.

A digital deep-towed multichannel streamer (52 traces @ 2m) has been developed and the feasibility of performing high-resolution (220-1050 Hz) multichannel seismic imaging in deep water has been demonstrated (Marsset et al., 2014). Yet, the seismic data acquired during early sea trials of this streamer did not allow to determine the P-wave velocity distribution as the altitude of the towed fish was kept conservatively high at 150 m above the sea floor.

One of the objectives of the GHASS project aims at studying the dynamics of gas hydrates and free gas associated with geological and climate processes (Ker et al., 2015). The GHASS project rests on a multidisciplinary approach including the fields of geotechnics, sedimentology and geochemistry. Such precise,

but local, measurements require in turn high resolution spatial information to correlate them. The deep towed seismic source SYSIF (Marsset et al., 2010), together with its digital multichannel streamer (Marsset et al., 2014), was therefore deployed to obtain high resolution seismic image as well as fine-scale P-wave velocity model.

The deep towed high resolution seismic source SYSIF (Marsset et al., 2010 ; Ker et al., 2010) and its digital multichannel streamer have already been described as well as the processing sequence of deep towed multichannel seismic data (Marsset et al., 2014). This contribution focuses on the determination of P-wave velocity distribution of gas and gas hydrates bearing sediments, highlighting the specific acquisition constraints and the dedicated processing sequence to get full benefit of pre-stack depth migration - velocity model building seismic imaging scheme .

II. METHODOLOGY

A. Acoustic source directivity

The ability to determine P-wave velocities from multichannel seismic data depends on the ratio between the source-receiver offset range and the depth of the seismic reflectors, i.e. a function of the incidence angle. In the framework of deep towed acquisition, this ratio can be easily expanded by lowering the system closer to the sea floor : the lower the altitude over the sea bottom, the larger the interval of incidence angles. For safety purposes considering the overall streamer length of 120 m, the minimum altitude with respect to the sea-bed is set to 50 m. Such a geometry allows to record incidence angles exceeding 45° for the upper sedimentary layers. Yet, one technical issue related to the acoustic source directivity arises for this approach in the particular framework of piezoelectric seismic sources.

The large frequency bandwidth of the JH220-6000 Janus-Helmholtz acoustic source (220-1050 Hz) is obtained by coupling of a mechanical resonance (Janus driver) and a fluid resonance (Helmholtz cavity) (Le Gall, 1999). Each transmitter has its own directivity, and the coupling between the two resonances results in a specific directivity for the transducer. The directivity of the JH220-6000 has been modeled using the ATILA software (figure 1), a finite element software designed for the analysis of mechanical 2D/3D structures hosting piezoelectric materials (Hennion et al., 1990 ; Le Gall & Marsset, 2007). Based on acoustic measurements acquired using OBH's (Ocean Bottom Hydrophone), Ker et al (2010) evaluated the main lobe of reflectivity of the JH220-6000 to 40° (@ -3dB), nevertheless the strong attenuation of the central frequencies (e.g. -8 dB @ 800 Hz @ 30°, figure 1) observed on the ATILA simulations suggests that the useful aperture is limited to 30°.

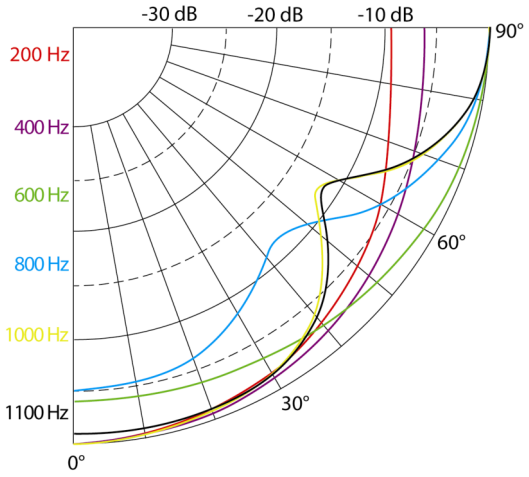

Fig. 1. : Relative directivity of the JH220-6000 piezoelectric transducer performed using ATILA software. 0°/90° corresponds respectively to the vertical axis and to the horizontal axis of the transducer.

The electric pilot source signal is a 100 milliseconds Linear FM (Linear Frequency Modulation) signal ranging from 220 to 1050 Hz. This initial signal is amplitude modulated taking into account the TVR (Transmit Voltage Response) of the transducer, in order to obtain an almost flat acoustic signal with a constant SL (Sound Level) of 196 dB ref 1µPa @ 1m over the entire frequency bandwidth in the nadir of the transducer. The "vertical" far field acoustic signature has been previously recorded (Ker et al., 2010). The "horizontal" far-field signature was recorded on the far hydrophone (in open water) during the GHASS cruise in order to assess the impact of the directivity of the transducer on the acoustic signal (figure 2, a-b). The classic processing sequence of linear FM signals involves performing either matching filter or deconvolution of the raw data with a known template in order to maximize the temporal resolution. The results of the deconvolution of the two signatures using the "vertical" signature as template clearly points out the incompatibility of this classic processing sequence for seismic data acquired with Janus-Helmholtz-like transducers as the source signature depends on the incidence angle (figure 2, c-d).

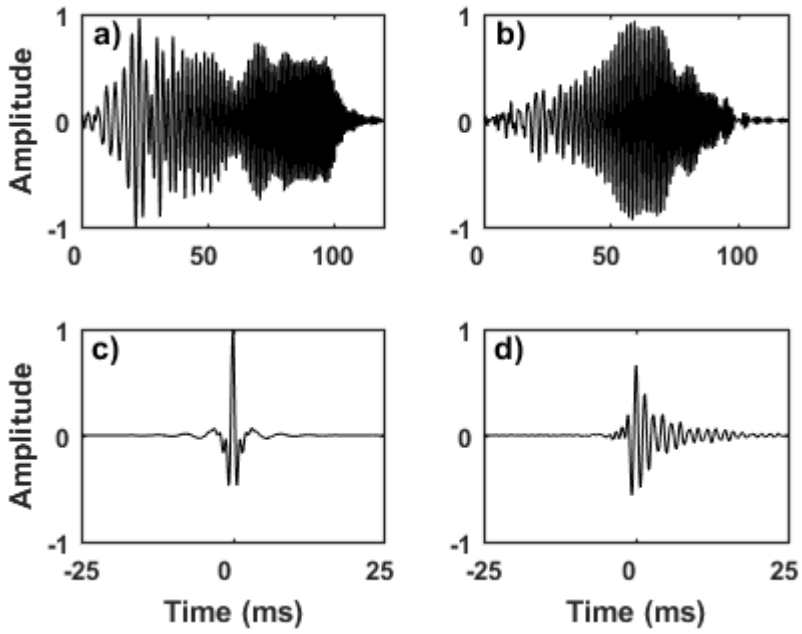

Fig. 2. : "Vertical" (a) and "horizontal" (b) acoustic signatures of the JH220-6000 transducer.
c) : Result of the deconvolution of the "vertical" signature (a) with the "vertical" signature (a).
d) : Result of the deconvolution of the "horizontal" signature (b) with the "vertical" signature (a)

B. Acoustic interferences

The zero offset travel time corresponding to the source/sea-bottom/receiver ray is to be 66 ms for an altitude of 50 meters (@ 1500 m/s) and therefore this ray will interfere with the direct arrival corresponding to the source/receiver ray. A processing step was therefore added, prior to source deconvolution, using STFT (short term Fourier transform) which allows to filter data in the Time-Frequency domain, a domain well adapted to Linear FM type signals (Allen, 1977).

The method was first applied on synthetic data (figure 3). The synthetic seismogram consists in the combination of a zero-delay "horizontal" signature with a 66 milliseconds delayed / 20 dB attenuation "vertical" signature thus mimicking a reflection on the sea bed with a 0.1 reflection coefficient for a monostatic acquisition. The synthetic seismogram is then transformed, taking advantage of STFT algorithm, in the time-trequency domain where the two signatures appear as separated signals. The modulus of the STFT corresponding to the direct arrival, i.e. "horizontal" signature, is then zeroed and the inverse STFT is performed to compute the processed seismogram back into the time domain. After deconvolution, the gain in S/N (signal to noise ratio) is evaluated to 18 dB on synthetic data.

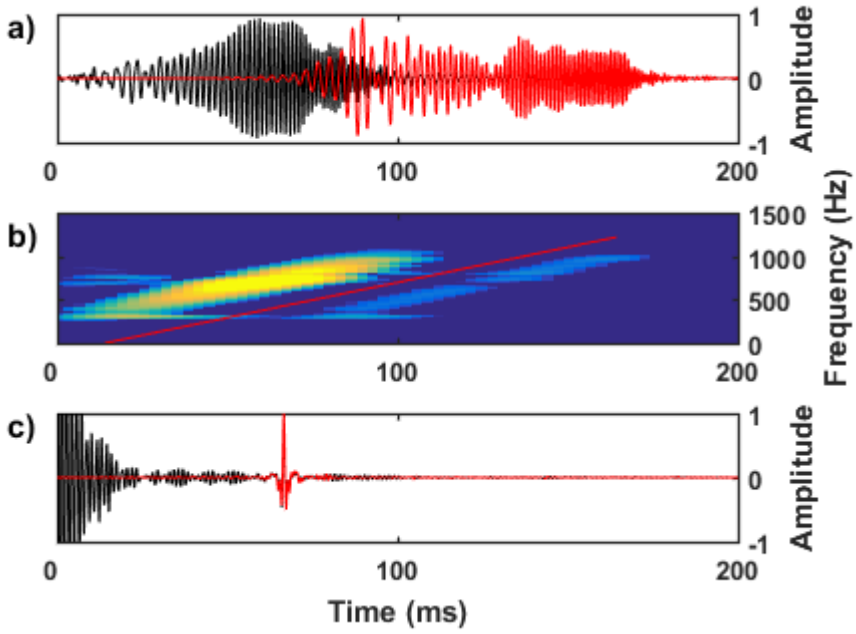

Fig. 3. : Signal processing sequence
a) : Raw synthetic seismogram (black/red curves without/with time-frequency filtering), data are normalized.
b) : STFT modulus of the synthetic seismograms, data left of the red line are muted. The red line corresponds to the slope of the linear frequency modulated signal.
c) : Synthetic seismogram after deconvolution (black/red curves without/with time-frequency filtering), data are normalized.

The former signal processing sequence was then applied on the SYSIF seismic data. Data are first deconvolved using the "horizontal" acoustic signature in order to precisely pick the direct arrivals (i.e. source-receiver ray) for each hydrophone. Raw traces are then time shifted to the direct arrival time of the first receiver so that filtering can use the same mask in the time-frequency domain for the entire data set. After filtering, data are shifted back to their original time and deconvolved with the proper template, i.e. "vertical" acoustic signature. The results are presented on figure 4 which illustrates the gain in S/N.

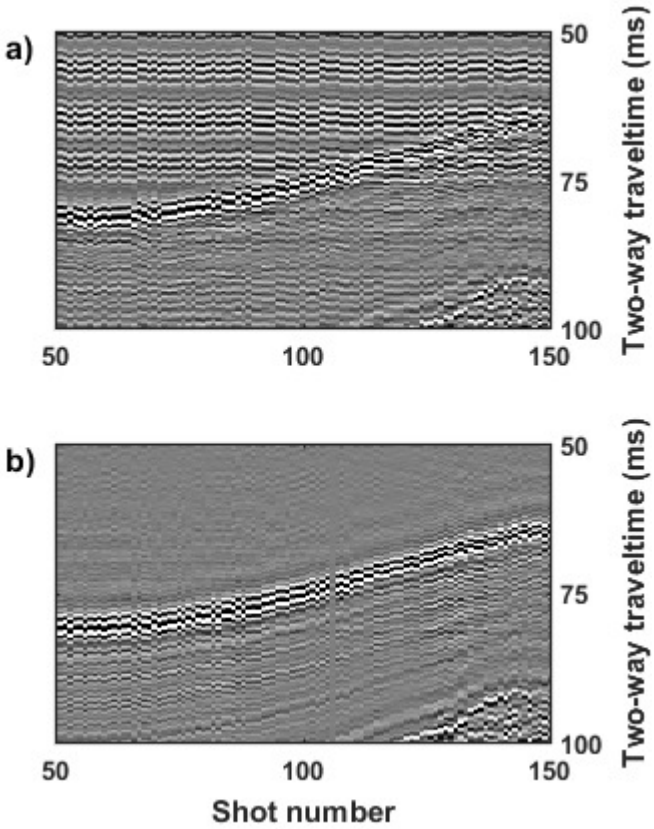

Fig. 4. : Signal processing sequence without (a) / with (b) time-frequency filtering of the direct arrival followed by deconvolution.

C. Positioning processing

Positioning is the key issue in seismic imaging processing where the calculation of travel times rests on the positions of the different source-receiver pairs. A relative error of one wavelength, i.e. ≈2 m for the mean wavelength of the JH220-6000 transducer, will prevent a proper focalization of the seismic events and therefore will lower the optimal resolution.

The streamer geometry is evaluated based on the hydrophones MEMS (Micro-Electro-Mechanical System) pitch and heading values. The geographic location of the source is ensured by an acoustic USBL (ultra short base line) (Marsset et al., 2014).

In order to evaluate the positioning accuracy, the theoretical sea bed reflection travel times were calculated using the streamer geometry together with a 10 m DTM (digital terrain model), obtained from a multibeam survey, in a 2D ray tracing in-house algorithm. The sea floor reflected travel times were picked on a CRG (common receiver gather) basis for all shots. The time differences between modeled and observed (picked) travel times for each hydrophone reveal a Gaussian distribution which allows the standard deviation to be evaluated after curve

fitting. The standard deviation for the different hydrophones ranges from 0.1 ms (≈0.15 m) to 0.7 ms (≈1.05 m) with an average value of 0.3 ms (≈0.45 m) well inside the accuracy requirements. The time differences between modeled and picked data are interpreted as "residual statics" and applied to the seismic data set.

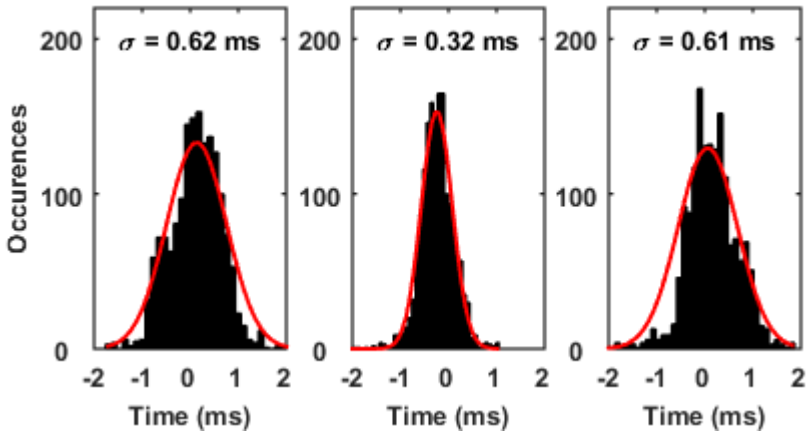

Fig. 5. : Distributions of the sea floor reflected arrival time differences between modeled and observed (picked) values. From left to right, hydrophones n° 1, 26 and 52 (line GHASS PL01PR02B).

III. VELOCITY DETERMINATION

The particular geometry of the acquisition where the source receiver geometry is perpetually changing, does not allow the seismic data to be processed in a “conventional” marine sequence: CMP (common mid point) sorting – (NMO) normal move out – stack (Asakawa et al., 2009). We adapted a pre-stack processing approach in order to take into account the real (X,Y,Z) positions of both sources and receivers in the imaging process.

The imaging process applies Kirchhoff depth migration to each CRG. The Green functions are calculated using the finite difference Eikonal equation solver from Podvin and Lecomte (1991). The source and receiver travel times are computed using 0.1 m * 0.1 m grid cells in order to take into account the high frequency content of the acoustic signal. The migrated traces are calculated every 1.0 meters which satisfy the aliasing limits for the JH220-6000 frequency bandwidth. The migration aperture is limited to 30° according to the directivity of the transducer.

The different migrated sections are then sorted into CIG (Common Image Gathers), i.e. to build an image of the same terrain location obtained from the different receivers. If the migrated traces of a CIG are identical for the different receivers, i.e. flat reflections along the offsets, this shows the validity of the velocity model. This approach is carried out in a layer-stripping iterative scheme to obtain, simultaneously, the variation of P-wave velocity with depth and the imaging result.

The selection of the "correct" velocity is presented through a simplified approach (migration velocity scan). Figure 6 presents a CIG migrated using different velocities. A number of selected horizons are picked.

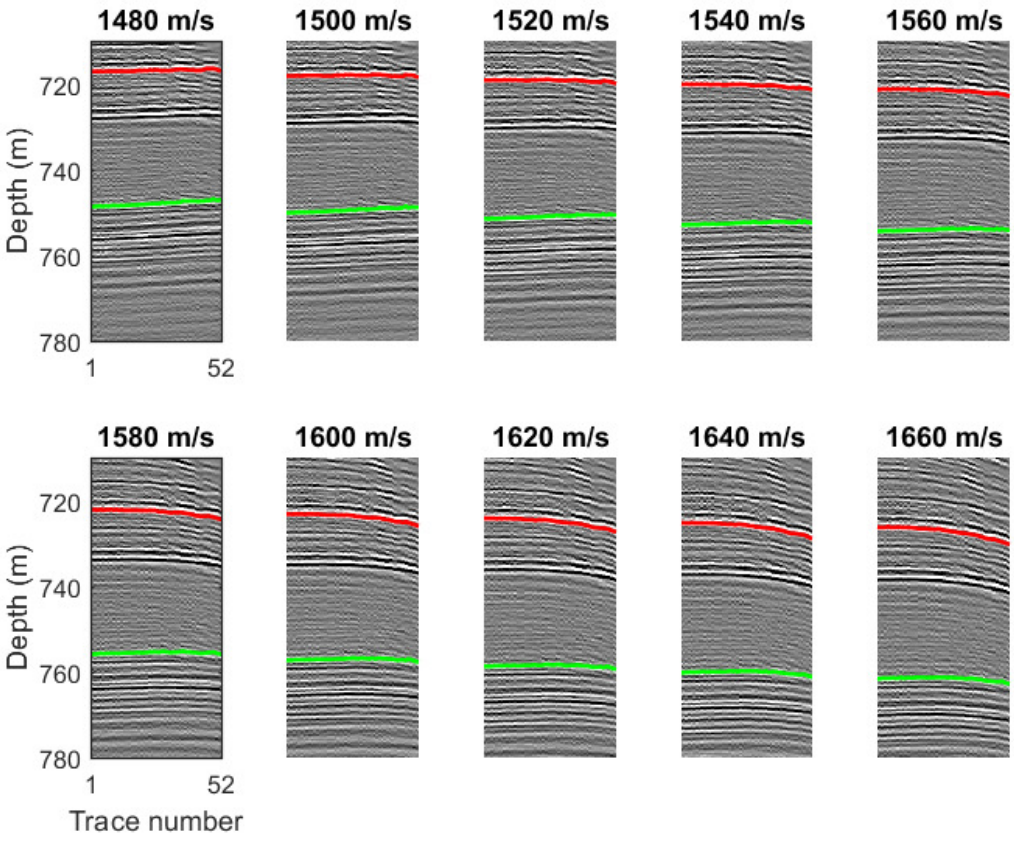

Fig. 6. : Migration velocity scan. An identical CIG obtained from different constant velocity migration. Selected horizons are picked.

The different horizons are then fitted with a second order polynomial. The first coefficient of the polynomial accounts for the "curvature", the second coefficient for the "linear trend". The correct velocity is selected where both the "curvature" and the "linear trend are reduced to zero (figure 7).

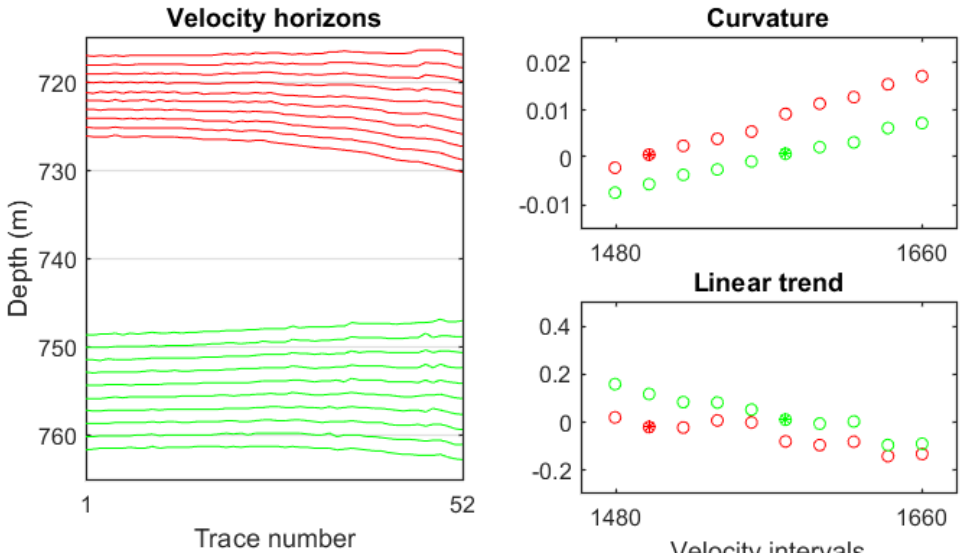

Fig. 7. : The selected velocity horizons are fitted with a second order polynomial. The correct velocity is selected where the "curvature" (1st polynomial coefficient) and the "linear trend" (2nd polynomial coefficient) are both reduced to zero (2nd velocity (1500 m/s) for the upper (red) layer, 6th velocity (1580 m/s) for the lower green) layer).

IV. RESULTS

SYSIF completed three dives during the GHASS cruise, corresponding to a total mileage of 230 miles (115 hours, 30 profiles) at an average speed of 2 knots (Ker et al., 2015). The altitude of the towed fish over the sea bottom was set to 100 meters in most cases in order to avoid interferences between direct and reflected arrivals. Two of the profiles were re-acquired with an altitude of 50 meters over the sea bed in order to better constrain the calculation of P-wave velocity.

A. Line PL01PR02B

The line was first acquired with an altitude of 100 meters (line PL01PR02). On board processing of this line underlines the presence of strong amplitude anomalies interpreted as a BSR (Bottom Simulating Reflector), a reflector which mimics the seabed reflection and which is presumably caused by gas hydrates bearing sediments overlying gassy sediments. As the presence of gas hydrates is likely to cause an increase in the P-wave velocity distribution, the line was re-acquired with an altitude of 50 meters and a shooting rate of one per 2.2 seconds.

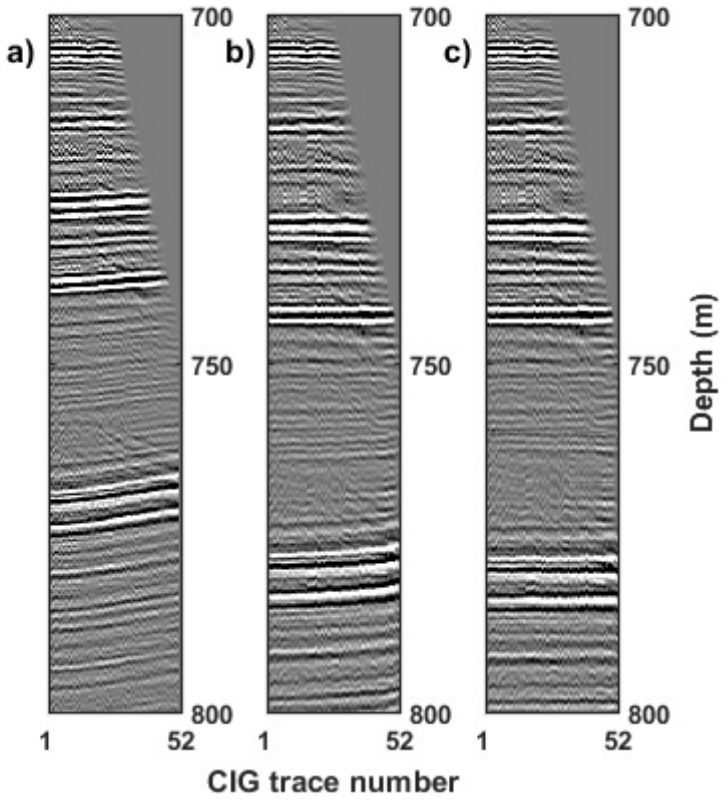

Fig. 8. : Common Image Gather (line PL01PR02B)
a) : One layer velocity model : Water velocity (1480m/s)
b) : Two layers velocity model : 1480m/s - 1700 m/s @ 720 meters
c) : Three layers velocity model : 1480m/s - 1700 m/s @ 720 meters - 1800 m/s @ 775 meters

The first iteration of the velocity analysis was performed with a constant (water) velocity of 1480 m/s derived from XCTD (expendable conductivity-temperature-depth) probe measurements (figure 8a). The seabed reflection appears flat on the CIG while deeper reflectors displays an upward curvature, characteristic of an increase of the P-wave velocity. The second iteration was performed using a two layers velocity model (figure 8b) with a 1700 m/s value. Eventually the third iteration used a three layers velocity model, adding an 1800 m/s layer down to the BSR (figure 8c).

The resolution enhancement associated to the velocity model in the final imagery result is obvious (figure 9a). The figure presents a comparison of the imagery results for the constant (water) velocity model (figure 9b) and the three layers velocity model (figure 9c), where the latter displays well focussed reflectors as well as sharp terminations of the amplitude anomalies.

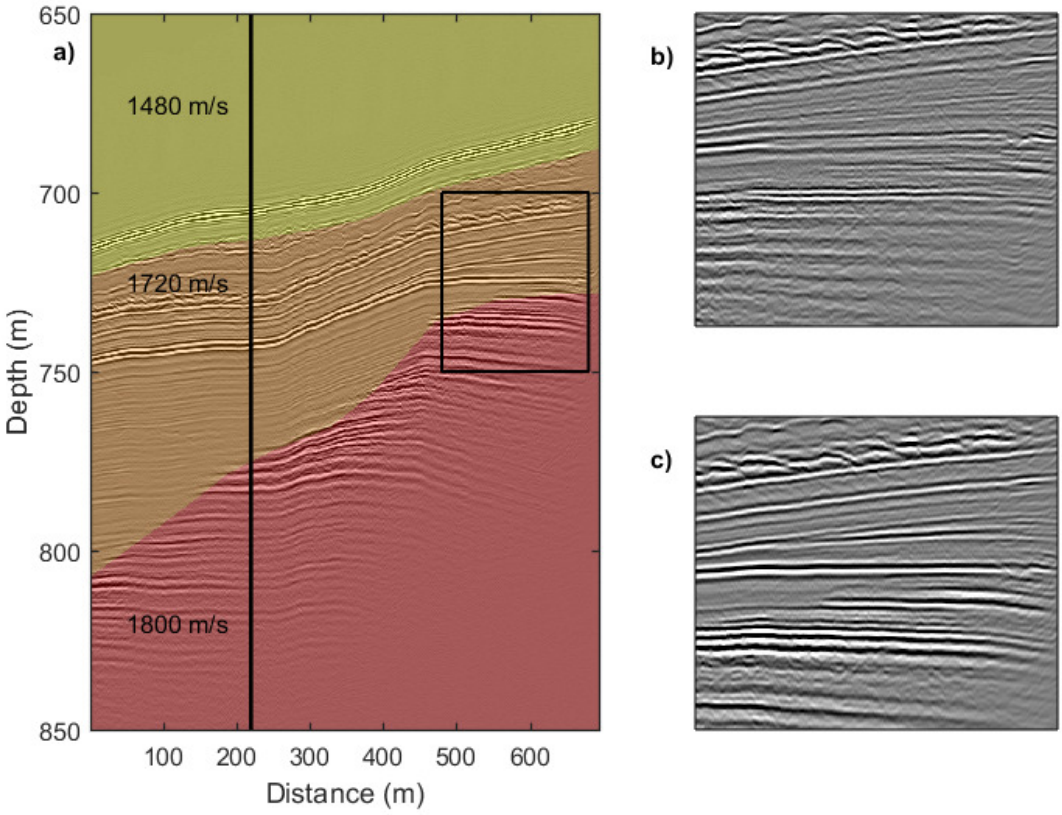

Fig. 9. : Imaging performance improvement
a): Regional line calculated with the three layers velocity model (green), the vertical red line corresponds to the position of CIG 210 of Fig. 8. The velocity model is superimposed.
b) : Imaging results of the red inset for the constant (water) velocity model
c) : Imaging results of the red inset for the three layers velocity model

B. Line PL03PR06

During the GHASS cruise, the water column was thoroughly monitored using multibeam technology with water columns record, in order to map possible offshore seeps (e.g. Dupre et al., 2015). The deep towed seismic line PL03PR06 was acquired over a major gas seep observed in the water column suggesting the presence of free gas in the sedimentary column (acquisition parameters : altitude = 50 m, shooting rate : one per 2.5 seconds).

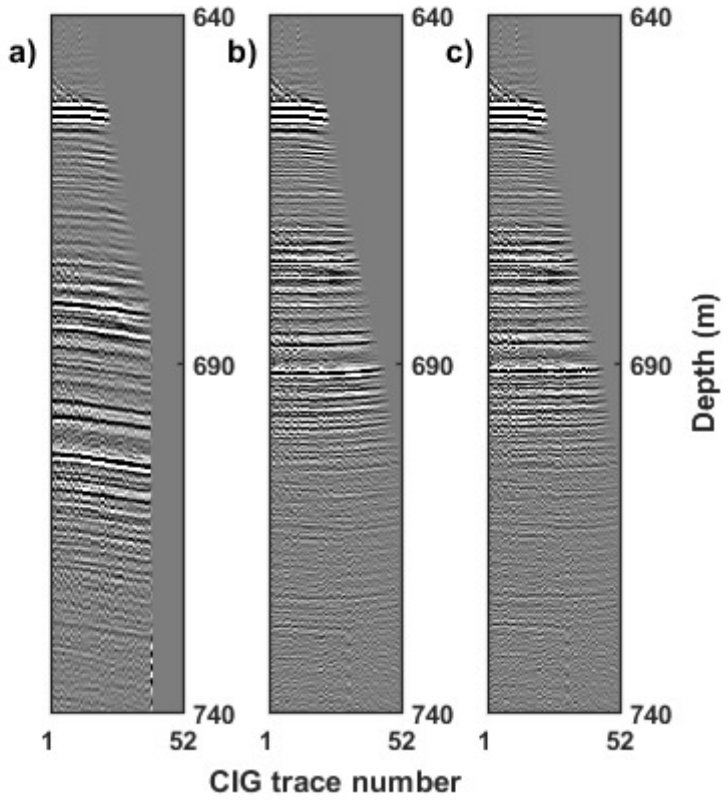

Fig. 10. : Common Image Gather
a): One layer velocity model : Water velocity (1480m/s)
b) : Two layer velocity model : 1480m/s - 1100 m/s @ 665 meters
c) : Three layer velocity model : 1480m/s - 1100 m/s @ 665 meters - 1250 m/s @ 680 meters

The first iteration of the velocity analysis was performed with a constant (water) velocity of 1480 m/s obtained from XCTD probing (figure 10a). The seabed reflection appears nearly flat on the CIG while deeper reflectors displays downward curvature, characteristic of a decrease of the P-wave velocity. The second iteration was performed with a two layers velocity model (figure 10b) with an 1100 m/s value. This model allows to flatten reflectors down to 680 meters but tends to overcorrect underlying reflectors, therefore, the third iteration uses a three layers velocity model, adding an 1200 m/s layer (figure 10c).

Again the gain in resolution associated to the velocity model in the final imagery result is clearly visible (figure 11a). The figure presents a comparison of the imagery results for the constant (water) velocity model (figure 11b) and the three layers velocity model (figure 11c), where the latter displays well focussed reflectors.

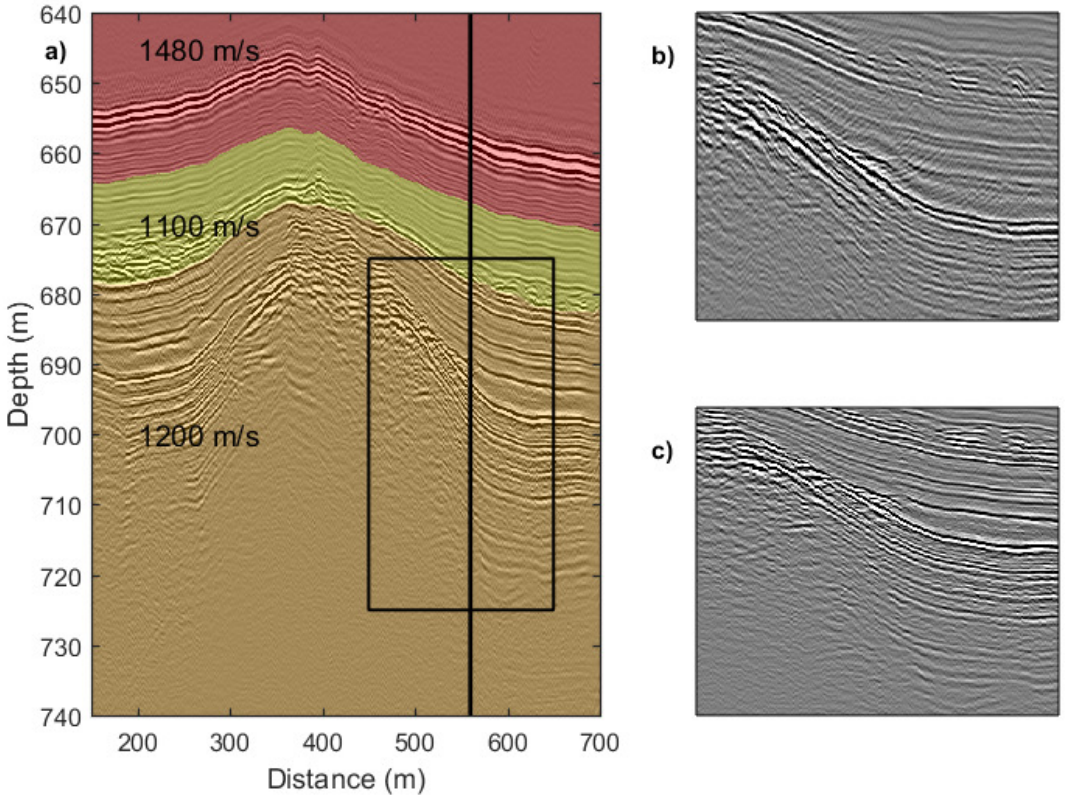

Fig. 11. : Imaging performance improvement
a) : Regional line calculated with the three layers velocity model (green), the vertical red line corresponds to the position of 560CIG of Fig. 10. The velocity model is superimposed.
b) : Imaging results of the red inset for the constant (water) velocity model
c) : Imaging results of the red inset for the three layers velocity model

V. DISCUSSION

The impact of the P-wave velocity distribution on the final vertical resolution was tentatively quantified on line PL03PR06. The average wavenumber spectrum of a selected part of the line for the constant and the three layers velocity models (figure 12a) are calculated (figure 12b). As a result, the central wavenumber is shifted from 2/3 m^{-1} (1.5 m) for the water velocity model to 1 m^{-1} (1 m) for the three layers velocity model.

An evaluation of the local gain in amplitude was performed on line PL01PR02B where reflectors were picked on the imaging results of the constant and three layers velocity model (figure 10 c-d). The average gain is evaluated to 7 dB for this reflector.

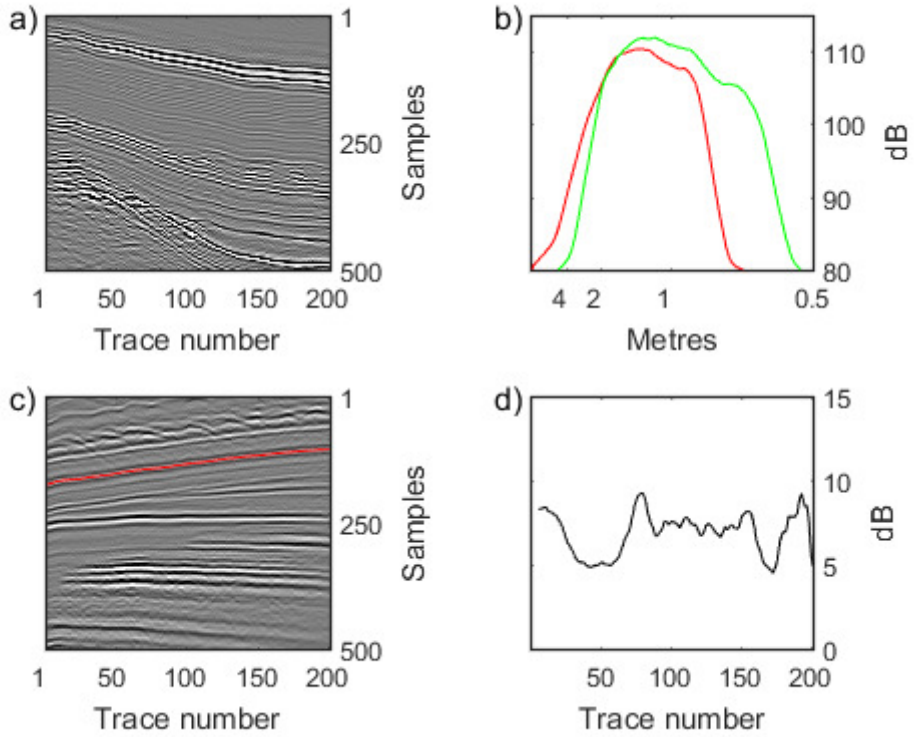

Fig. 12. : Imaging performance improvement
a) : Line PL03PR06 (three layers velocity model) and b) : corresponding average wavenumber spectra (red : constant velocity model, green : three layers velocity model)
c) : Line PL01PR02B (three layers velocity model) and d) : amplitude ratio on a given reflector using constant and three layers velocity model.

In this contribution, we used Kirchhoff migration to perform seismic depth imaging of High Resolution deep towed seismic data. Kirchhoff migration is an efficient algorithm, easy to implement with fast calculation times. Nevertheless, this algorithm requires smooth variations of the velocity field and thus, in theory, it is not able to cope with sharp interfaces as the seafloor interface or the gas hydrate / free gas interface. Migration methods based on (FD) finite-difference migration are more suited to deal with fast space variation of the velocity field, e.g. Ristow and Rühl, 1994, Plessix and Mulder, 2004 ; Brossier et al., 2008). These methods allows to define very accurately the velocity field but have a very high computational cost. The algorithms associated to FD migration will be adapted to the specific deep-towed seismic geometry together with the development of anti-aliasing and over-sampling techniques in order to increase the resolution of the final velocity model.

VI. CONCLUSION

The ability to perform high-resolution velocity analysis using a deep towed multichannel streamer has been demonstrated, based on the data set acquired during the GHASS cruise on the Romanian side of the Black sea. The obtained P-wave velocity distribution is in agreement with the preliminary geological interpretation with 1)

an increase of the velocities above a BSR (PL01PR02B) and 2) a decrease of these velocities associated with the presence of free gas assessed by acoustic flares in the water column (PL03PR06). The improvement in seismic imaging strongly supports the validity of the velocity results.

The GHASS project will be the first project to benefit from the spatial resolution achieved in deep towed High Resolution seismic imaging. The P-wave velocity distribution extracted from seismic data has now to be compared with in situ measurements obtained in the fields of geotechnics (velocity probe), sedimentology and geochemistry (gas nature/content). GHASS cruise data will then form a unique data set to understand the dynamics of gas hydrates and free gas in the geological and climate processes.

Acknowledgments:

The GHASS cruise was funded by French research institute for exploitation of the sea (Ifremer).

The development of the multichannel streamer was funded by Institut Carnot Ifremer EDROME.

The authors are indebted to the scientific party and to the crew of the GHASS cruise onboard French R/V "Pourquoi Pas ?".

References:

Allen, J. B., 1977. Short Time Spectral Analysis, Synthesis and Modification by Discrete Fourier Transform. IEEE Transactions on Acoustics, Speech and Signal Processing. ASSP-25 (3), 235-238.

Brossier, R., Virieux, J., and Operto, S. 2008, Parsimonious finite-volume frequency-domain method for 2D P-SV-wave modeling, Geophysical JournalInternational, 175(2), 541-559

Chapman, N.R., J.F. Gettrust, R. Walia, D. Hannay, G.T. Spence, W.T. Wood and R.D. Hyndman, 2002, High Resolution deep-towed multichannel seismic survey of deep sea gas hydrates off western Canada, Geophysics, 67, 1038-1047

Dupré, S., C. Scalabrin, C. Grall, J. M. Augustin, P. Henry, A. M. C. Sengör, N. Görür, M. N. Cagatay, and L. Géli , 2015, Tectonic and sedimentary controls on widespread gas emissions in the Sea of Marmara: Results

from systematic, shipborne multibeam echo sounder water column imaging, J. Geophys. Res. Solid Earth, 120(5), 2891-2912.

Gettrust, J.F., W. Wood, and S. Spychalski, 2004, High-resolution MCS in deepwater, The leading Edge, 23, 374-377.

He, T., G. Spence, W. Wood, M. Riedel, and R. Hyndman, 2009, Imaging a hydrate-related cold vent offshore Vancouver Island from deep-towed multichannel seismic data, Geophysics, 74(2), B23-B26.

Helgerud M. B., J. Dvorkin, and A. Nur, 1999, Elastic-wave velocity in marine sediments with gas hydrates : Effective medium modeling, Geophysical Research Letters, 26(13), 2021-2024.

Hennion, A.C., Bossut, R., and Decarpigny, J.N., 1990, Analysis of the scattering of a plane acoustic wave by a periodic elastic structure using the finite element method: Application to compliant tube gratings, Journal of the Acoustical Society America, 87(5), 1861-1870

Ker, S., B. Marsset, S. Garziglia, Y. Le Gonidec, D. Gibert, M. Voisset, and J. Adamy, 2010, High-resolution seismic imaging in deep sea from a joint deep-towed/OBH reflection experiment : application to a Mass Transport Complex offshore Nigeria, Geophysical Journal International, 182(3), 1524-1542.

Ker S., V. Riboulot and Ghass Cruise Team, 2015, GHASS cruise report.

Le Gall Y., and B. Marsset, 2007, Développements électroacoustiques en sismique marine Très Haute Résolution. Acoustique & Techniques, (48), 17-22

Marsset B., E. Menut, S. Ker, Y. Thomas, J. P. Regnault, P. Leon, H. Martinossi, L. Artzner, D. Chenot, S. Dentrecolas, B. Spychalski, G. Mellier, and N. Sultan, 2014, Deep-towed High Resolution multichannel seismic imaging, Deep Sea Research Part I : Oceanographic Research Papers, 93, 83-90.

Marsset T., B. Marsset, S. Ker, Y. Thomas, and Y. Le Gall, 2010, High and very high resolution deep-towed seismic system: Performance and examples from deep water geohazard studies, Deep-sea Research Part I-oceanographic Research Papers, 57(4), 628-637.

Plessix, R.-E. and Mulder, W.A., 2004, Frequency-domain finite-difference amplitude-preserving migration, Geophysical Journal International, 157(3), 957-987

Podvin P. and I. Lecomte, 1991, Finite difference computation of traveltimes in very contrasted velocity models. A massively parallel approach and its associated tools, Geophysical Journal International, 105, 271–284.

Ristow D. and Rhül, T., 1994, Fourier finite difference migration, Geophysics, 55(4), 410 421.

Wood, W., J. F. Gettrust, and S. E. Spychalski, 2003, A new deep-towed, multi-channel seismic system, Sea Technology, 44(9), 44-49.

Wood, W. T., P. Hart, D. Hutchinson, N. Dutta, F. Snyder, R. Coffin, and J. F. Gettrust, J., 2008, Gas and gas hydrate distribution around seafloor seeps in Mississipi Canyon, Northern Gulf of Mexico, using multi-resolution seismic imagery, Marine and Petroleum Geology, 25(9), 952-959.